Bichromatic Rabi Control of Semiconductor Qubits

John, Valentin; Borsoi, Francesco; György, Zoltán; Wang, Chien An; Széchenyi, Gábor; Van Riggelen-Doelman, Floor; Lawrie, William I.L.; Hendrickx, Nico W.; Sammak, Amir; Scappucci, Giordano

Important note
To cite this publication, please use the final published version (if applicable).
Please check the document version above.

Bichromatic Rabi Control of Semiconductor Qubits

Valentin John[1,*] Francesco Borsoi[1,*] Zoltán György[2,*] Chien-An Wang[1] Gábor Széchenyi[2]
Floor van Riggelen-Doelman[1] William I. L. Lawrie[1] Nico W. Hendrickx[1] Amir Sammak[3]
Giordano Scappucci[1] András Pályi[4,5] and Menno Veldhorst[1]

[1]*QuTech and Kavli Institute of Nanoscience, Delft University of Technology,*
P.O. Box 5046, 2600 GA Delft, Netherlands
[2]*ELTE Eötvös Loránd University, Institute of Physics, H-1117 Budapest, Hungary*
[3]*QuTech and Netherlands Organisation for Applied Scientific Research (TNO),*
Stieltjesweg 1, 2628 CK Delft, Netherlands
[4]*Department of Theoretical Physics, Institute of Physics, Budapest University of Technology and Economics,*
Műegyetem rakpart 3, H-1111 Budapest, Hungary
[5]*MTA-BME Quantum Dynamics and Correlations Research Group, Budapest University of Technology and Economics,*
Műegyetem rakpart 3, H-1111 Budapest, Hungary

Electrically driven spin resonance is a powerful technique for controlling semiconductor spin qubits. However, it faces challenges in qubit addressability and off-resonance driving in larger systems. We demonstrate coherent bichromatic Rabi control of quantum dot hole spin qubits, offering a spatially selective approach for large qubit arrays. By applying simultaneous microwave bursts to different gate electrodes, we observe multichromatic resonance lines and resonance anticrossings that are caused by the ac Stark shift. Our theoretical framework aligns with experimental data, highlighting interdot motion as the dominant mechanism for bichromatic driving.

Introduction.—Spin qubits based on semiconductor quantum dots represent a promising platform for quantum computing owing to their small qubit footprint, long coherence times, and compatibility with semiconductor manufacturing techniques [1,2]. However, the present control of spin qubit devices relies on a brute force approach, where each qubit is individually connected to at least one control line. This approach poses a significant challenge for scaling to larger systems and is affecting current progress [3,4]. Multiplexing strategies will most likely become essential and this has been the motivation for various proposals, such as crossbar arrays with shared control [5,6]. Executing quantum algorithms requires selective quantum control, but its implementation in large qubit arrays poses significant challenges. Recently, the concept of bichromatic spin resonance has been proposed to offer addressable microwave control in qubit crossbar architectures [7]. In this approach, two microwave tones with frequencies f_w and f_b are utilized. These tones are applied to the word and the bit line of the crossbar array, respectively. By exploiting the nonlinearity of electric dipole spin resonance (EDSR) [8–16], rotations of a qubit with Larmor frequency of $|f_w \pm f_b|$ at the intersection of the two lines [Fig. 1(a)] can be targeted. This operation scheme presents new opportunities for both spatially selective qubit addressing and gate parallelization [7]. Analogous two-photon processes have been utilized in

Rydberg-atom processors [17,18] and superconducting qubits [19] to optimize qubit performance.

Here, we investigate experimentally and theoretically the bichromatic driving of semiconductor spin qubits in a 2-qubit system defined in a strained germanium quantum well. We find that both qubits can be coherently driven by mixed frequency signals, including the sum and difference of the corresponding frequencies. We investigate the occurrence of resonance anticrossings in EDSR spectroscopy maps, which originate from the Autler-Townes (also known as ac Stark) shift of a photon-dressed spin transition. Additionally, we introduce a model that reveals the importance of spin-conserving and spin-flip tunneling terms in bi- and monochromatic EDSR.

Results.—We investigate bichromatic driving of spin qubits in a 2-qubit system within a 4-qubit germanium quantum processor [Figs. 1(b) and 1(c)] [20,21]. By tuning the electrostatic potential using plunger and barrier gates, we confine a single-hole quantum dot underneath each of the four plungers $P1$–$P4$ and define virtual gate voltages $vP1$–$vP4$ based on $P1$–$P4$ to achieve independent control (Supplemental Material Note 1 [22]). We focus on the spin qubits $Q1$ and $Q2$, while $Q3$ and $Q4$ remain in their ground state. We furthermore define the detuning voltage $\epsilon_{12} = vP1-vP2$ [29].

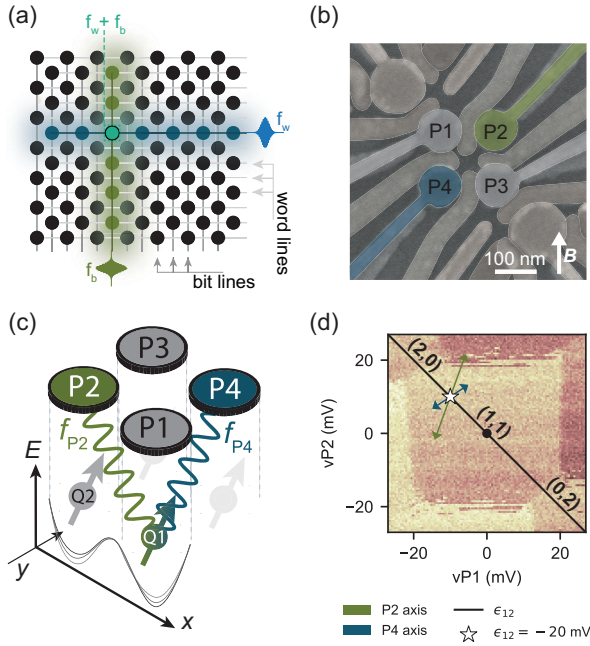Figure 1(d) displays the charge stability diagram of the double quantum dot system, obtained through

FIG. 1. Bichromatic control of a spin qubit. (a) Bichromatic driving in a crossbar architecture. (b) False-color scanning electron microscopy of a 2×2 germanium quantum dot device, nominally identical to the one used here. (c) Illustration of the 4-qubit processor. We operate $Q1$ and $Q2$ with microwave bursts applied to $P2$ and $P4$. We model qubit rotations via ac detuning modulation (sketched potential). (d) Charge stability diagram of the double quantum dot illustrating the (1,1) charge sector and the detuning ϵ_{12} axis (black line). The white star indicates the gate voltages used for the qubit manipulation stage. The green and blue arrows indicate the displacement within the $vP1, vP2$ framework, when applying a microwave burst on $P2$ and $P4$, showcasing the different orientation of the driving fields. The displayed length of the arrows is proportional to the amplitude of the signal at the device, amplified by a factor of 5 for visibility.

rf-reflectometry charge sensing [30]. The device is operated in an in-plane magnetic field of 0.675 T, resulting in qubit frequencies of $f_{Q1} = 1.514$ and $f_{Q2} = 2.649$ GHz. To investigate the bichromatic driving approach, we follow the pulse protocol outlined in Fig. 2(a). We initialize the $Q1$, $Q2$ qubits in the $|{\downarrow}{\downarrow}\rangle$ state by adiabatically pulsing ϵ_{12} from the (0,2) to the (1,1) charge state via the spin-orbit induced anticrossing. Next, we manipulate the spins by two simultaneous microwave pulses on plunger gates $P2$ and $P4$, with a duration t_p and microwave frequencies f_{P2} and f_{P4}. We perform such two-tone qubit manipulation at the voltage point indicated in Fig. 1(c) corresponding to $\epsilon_{12} = -20$ mV. Finally, we return to the (0,2) charge sector and perform readout using latched Pauli spin blockade [20].

The 2D EDSR spectroscopy in Fig. 2(b) reveals resonance lines from mono- and bichromatic spin excitations. Monochromatic qubit transitions labeled as $Q1^{P2}$, $Q1^{P4}$,

$Q2^{P2}$, and $Q2^{P4}$ (with the superscript defining the driving plunger gate) are observed as vertical and horizontal lines at the corresponding Larmor frequencies. Bichromatic excitations appear as tilted resonance lines, with negative (positive) slopes indicating the frequency sum (difference) matching the qubit Larmor frequency. Three-photon bichromatic excitations can also be observed when a combination of two photons with the same frequency and a third one with a different frequency match the qubit Larmor frequency.

Figures 2(c) and 2(d) depict the expected resonance lines considering the individual resonance frequencies of the two qubits. The qubits exchange interaction resulting from interdot tunneling (55 MHz at $\epsilon_{12} = -20$ mV, see Supplemental Material Note 4 [22]) is taken into account. To label the Larmor frequency of qubit i when qubit j is in the excited state, we use the notation Qi_- (with $i, j \in \{1, 2\}$ and $i \neq j$). The monochromatic transition from $|{\downarrow}{\downarrow}\rangle$ to $|{\uparrow}{\uparrow}\rangle$ driven by $P4$ is then denoted as $(Q1 + Q2_-)^{P4}$. A bichromatic transition can be visualized as a two-step process via a virtual state, as illustrated in Fig. 2(e). Following perturbation theory, bichromatic spin transitions are activated thanks to spin-conserving (t) and spin-flipping (Ω) tunneling terms, which hybridize the four possible spin states with the $S(2, 0)$ state, as discussed below and in Supplemental Material Note 8 [22].

We analyze three resonance lines [dashed lines in Fig. 2(b)] resulting from bichromatic rotation of $Q1$ and $Q2$. The bichromatic $Q1$ spin resonance ($Q1^{-P2,P4}$) occurs when the frequency difference matches the $Q1$ Larmor frequency. Similarly, $Q2$ exhibits bichromatic resonance lines from both frequency difference ($Q2^{-P2,P4}$) and frequency sum ($Q2^{P2,P4}$). The bichromatic spin resonance $Q1^{P2,P4}$ is not investigated due to the presence of a high-pass filter (Supplemental Material Note 6 [22]). The conditions for the three studied bichromatic qubit rotations are $Q1^{-P2,P4}$, $f_{P4} - f_{P2} = f_{Q1}$; $Q2^{-P2,P4}$, $f_{P4} - f_{P2} = f_{Q2}$; and $Q2^{P2,P4}$, $f_{P4} + f_{P2} = f_{Q2}$. At these frequency combinations, we also achieve coherent bichromatic qubit rotations with a Rabi frequency exceeding 1 MHz, as we demonstrate in Figs. 2(f) and 2(g) and Supplemental Material Fig. 4 [22].

At the intersection of specific resonance lines [see Fig. 2(b)], we also observe anticrossings (labeled as ACn with $n \in \{1, \ldots, 5\}$ in Figs. 2(c) and 2(d). In Fig. 3, we analyze the evolution of the two bichromatic spin resonances, $Q2^{-P2,P4}$ and $Q2^{P2,P4}$, in the frequency plane. We vary the two microwave frequencies together to follow the two resonance lines, using Δf_{P2} in the range of $[-40, 40]$ MHz centered around the bichromatic resonance. This procedure allows one to monitor in detail the $Q2$ bichromatic spin resonance within the boxed areas indicated in Fig. 2(b). The bichromatic resonance aligns with
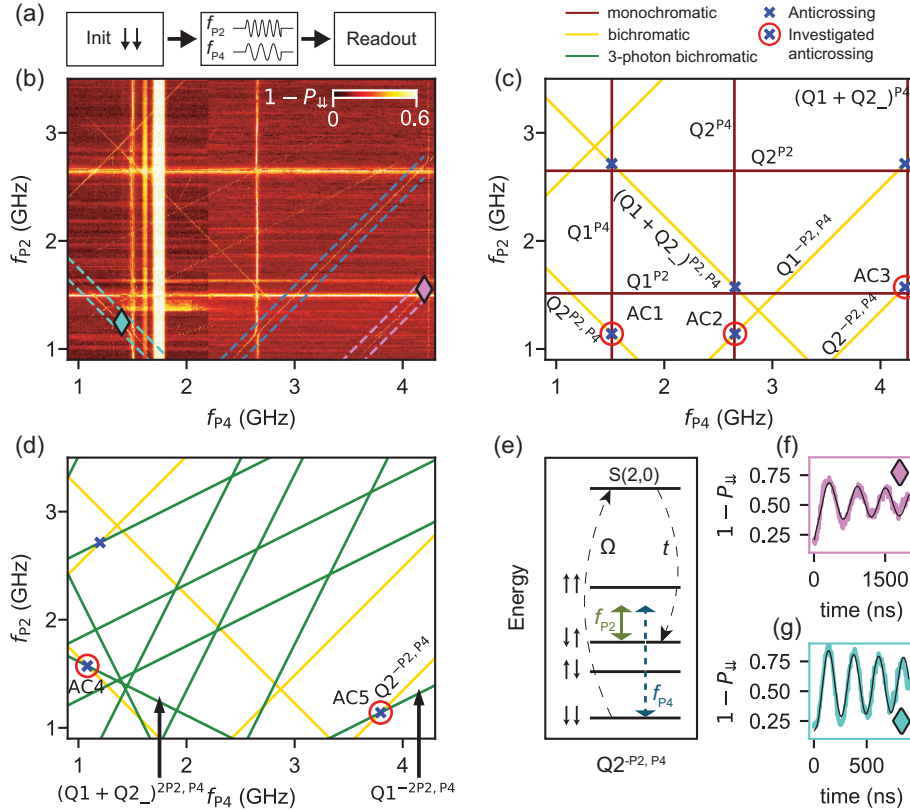
FIG. 2. Bichromatic EDSR spectroscopy. (a) Bichromatic control sequence. (b) Single-shot probability versus f_{P4} and f_{P2}, at $\epsilon_{12} = -20$ mV. We include three turquoise, blue, and purple dotted lines to enclose the bichromatic resonances of $Q2^{P2,P4}$, $Q1^{-P2,P4}$, and $Q2^{-P2,P4}$, respectively. The broad vertical excitation at $f_{P4} \sim 1.8$ GHz is associated with a transmission resonance in the lines, not to a spin transition. (c),(d) Monochromatic, bichromatic, and three-photon bichromatic excitations in the 2D frequency plane, as predicted by theory. (e) Energy diagram of a two-spin system with finite exchange and finite magnetic field. The green and blue arrows represent the applied microwave frequencies f_{P2} and f_{P4}, when driving the $Q2^{-P2,P4}$ transition. Driven spin-flipping processes originate from higher-order processes via the $S(2,0)$ state involving the spin-conserving tunneling term t and spin-flip tunneling term Ω. (f),(g) Coherent Rabi oscillations of the $Q2^{-P2,P4}$ and $Q2^{P2,P4}$ bichromatic transition. The corresponding f_{P2} and f_{P4} frequencies are indicated with the purple and turquoise diamonds in (b).

the expected value of $\Delta f_{P2} = 0$ for most of the frequency range. However, significant anticrossings occur when the resonance intersects with other qubit transitions. Examples of these anticrossings are observed at specific frequencies and are labeled as AC5, AC3 (for $Q2^{-P2,P4}$) and AC4, AC1 (for $Q2^{P2,P4}$).

The appearance of anticrossings in the frequency plane, such as AC3 in Fig. 3(a), result from resonant driving of mono- and bichromatic transitions from the $|\downarrow\downarrow\rangle$ state to higher (1,1) states. As shown in Figs. 3(e) and 3(f), AC3 involves three resonant processes: the bichromatic transition $|\downarrow\downarrow\rangle \leftrightarrow |\downarrow\uparrow\rangle$, the monochromatic $P4$ drive $|\downarrow\downarrow\rangle \leftrightarrow |\uparrow\uparrow\rangle$, and the monochromatic $P2$ drive $|\downarrow\uparrow\rangle \leftrightarrow |\uparrow\uparrow\rangle$. Because of the greater driving efficiency of $P2$ compared to $P4$ [see projected amplitudes in Fig. 1(c)], the dominant transition is $|\downarrow\uparrow\rangle \leftrightarrow |\uparrow\uparrow\rangle$ (Supplemental Material Note 8 [22]).

Driving via $P2$ dresses up the spin states $|\downarrow\uparrow\rangle$ and $|\uparrow\uparrow\rangle$ with microwave photons. In the rotating frame, where these

states are degenerate in the absence of $P2$ driving, the eigenstates become dressed in the form $[(|\downarrow\uparrow\rangle \pm |\uparrow\uparrow\rangle)/\sqrt{2}]$, and the corresponding eigenvalues exhibit a splitting set by the Rabi frequency. In this context, dressing refers to the coherent interaction between the electromagnetic field and the spin system, resulting in entangled states of spins and photons becoming the eigenstates of the coupled system.

This effect, known as the Autler-Townes effect or ac Stark shift, has been observed in quantum optics and in strongly driven superconducting qubits [31,32]. It is at the basis of control strategies for highly coherent solid-state qubits [33]. In particular, the continuous driving can decouple the spin from background magnetic field noise and thus extend their coherence [34,35].

Because of the Autler-Townes effect, the resonance frequencies of the two weaker transitions ($|\downarrow\downarrow\rangle \leftrightarrow |\downarrow\uparrow\rangle$ and $|\downarrow\downarrow\rangle \leftrightarrow |\uparrow\uparrow\rangle$) are shifted by the Rabi frequency of the strongly driven $|\downarrow\uparrow\rangle \leftrightarrow |\uparrow\uparrow\rangle$ transition, resulting in the

anticrossing between the resonance lines [AC3 in Figs. 3(a) and 3(b)].

We use a two-spin qubit Hamiltonian to model our system and gain a quantitative understanding. The model considers the lowest orbital in each dot, including four states in the (1,1) charge regime, as well as the (0,2) and (2,0) singlet states. Spin-conserving and spin-flip tunneling between the quantum dots are also included, with a coupling strength of t for spin-conserving transitions and Ω for spin-flip transitions (Supplemental Material Note 8A [22]). Despite neglecting additional electrical g-tensor modulations [2,36], this minimal model successfully explains electrically driven spin transitions via ac modulation of the detuning voltage using both mono- and bichromatic resonance techniques. Here, spin dynamics occur through virtual transitions between the (1,1) spin states and the (0,2) and (2,0) singlet states, mediated by the spin-conserving and spin-flipping terms, as shown in Fig. 2(e).

Our model provides an explanation for the observed resonance crossings and anticrossings in Figs. 3(a) and 3(c). Furthermore, by analyzing the five anticrossings AC1–AC5 using Floquet theory, as discussed in Supplemental Material Note 8C [22], we estimate the spin-conserving and spin-flip tunneling energies to be on average $t = (18.1 \pm 1.9)$ and $\Omega = (14.3 \pm 2.4)$ μeV (Supplemental Material Note 8F [22]).

To verify our theoretical description, we investigate the dependence of the $Q1^{-P2,P4}$ resonance anticrossing on the detuning voltage. Experimental data and the expected detuning dependence from the model are shown in Fig. 4. In the model, we use the average tunneling amplitudes and vary the detuning voltage. Moreover, we utilize an estimated detuning lever arm of $\alpha = 0.0917$ eV/V and quantum dot charging energy of $U = 2.56$ meV (Supplemental Material Note 8B [22]). Our theoretical model accurately captures the diminishing size of the anticrossing as the detuning approaches $\epsilon_{12} \sim 0$. Both the bi- and monochromatic resonance lines fade, indicating a reduced efficiency as detuning approaches zero. This is consistent with our model, since the transitions take place via the $S(0,2)$ and $S(2,0)$ states and in the high detuning limit the transition through $S(0,2)$ dominates the driving. At zero detuning, the two contributions become equal, while the Rabi frequency has a minimum.

The diminished efficiency of bichromatic operations near the charge-symmetry point supports the fundamental role of virtual interdot transitions as the underlying driving mechanism (Supplemental Material Note 3 [22]). In Supplemental Material Note 8D, we discuss the limitations of our model
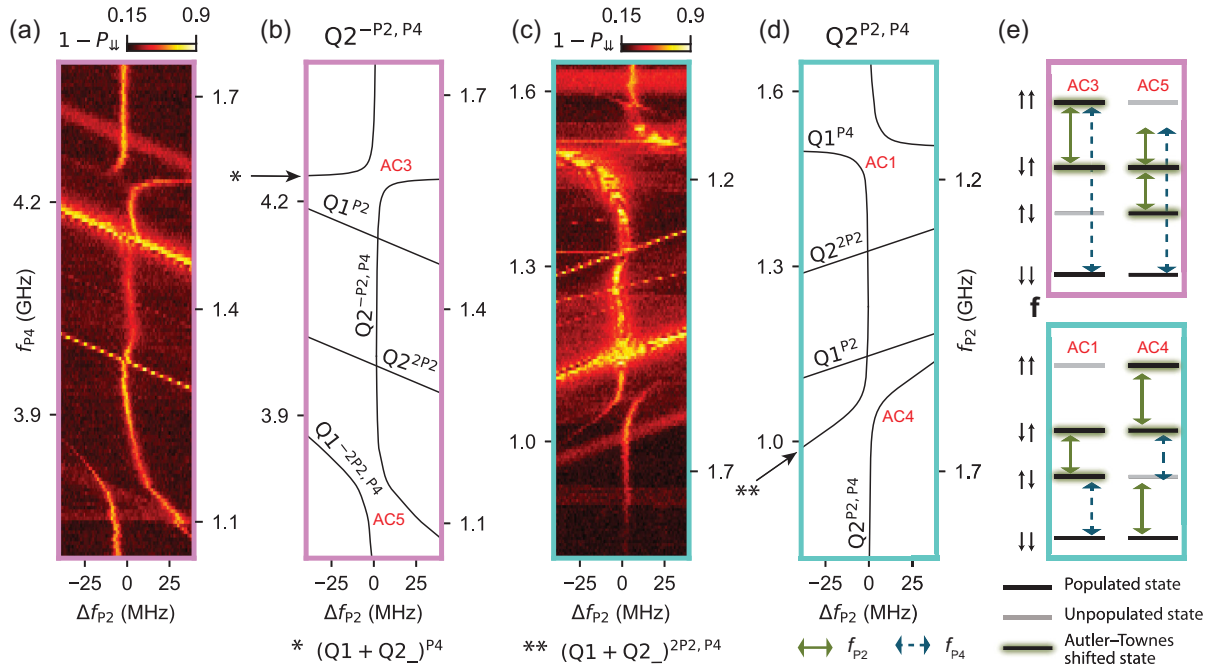

FIG. 3. Modeling the frequency anticrossings due to the Autler-Townes effect. (a),(c) Single-shot probabilities $(1 - P_{\downarrow\downarrow})$ in a frequency range around the bichromatic $Q2^{-P2,P4}$ and $Q2^{P2,P4}$ resonance conditions, respectively. These scans are higher-resolution measurements along the color-coded diagonals enclosed by two dashed lines in Fig. 2(b). Vertical lines of Fig. 2(b) appear horizontal, and horizontal lines appear slightly tilted [as can be seen with $Q1^{P2}$ and $Q1^{P4}$ in (d)]. The values on the f_{P2} axes are valid at $\Delta f_{P2} = 0$. (b),(d) Calculated transitions nearby the $Q2^{-P2,P4}$ and $Q2^{P2,P4}$ resonances. (e),(f) Illustration of the driven transitions at the four anticrossings. Strong driving via $P2$ induces a photon-dressed spin transition.
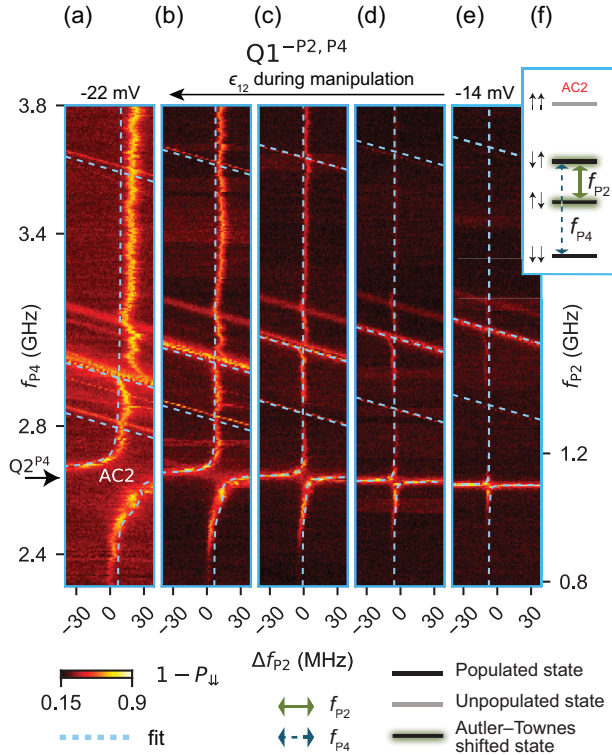
FIG. 4. Detuning dependence of the frequency anticrossings. (a)–(e) Bichromatic spectroscopy around the $f_{Q1} = f_{P4} - f_{P2}$ resonance versus detuning voltage. The anticrossing AC2 originates from strong driving of the $|\uparrow\downarrow\rangle \to |\downarrow\uparrow\rangle$ transition with $P2$ via the Autler-Townes shift. The AC2 frequency gap narrows down as a function of detuning voltage due to suppressed virtual transition from the (1,1) to the (2,0) charge state. We overlay the transition lines expected from theory. (f) Driven transitions at AC2, displaying the four lowest states from Fig. 2(c).

and suggest that additional mechanisms, such as EDSR induced by g-tensor modulation, may be necessary to fully interpret all experimental observations [37–39].

Conclusions.—Electric dipole spin resonance has enabled high-fidelity quantum gates on individual qubits, but a key challenge is the development of advanced operations for scalable control. Here, we have established bichromatic control of spin qubits and turned challenges in EDSR [14] into an opportunity for addressable qubit control in larger arrays. Moreover, we showed the relevance of interdot motion in obtaining bi- and monochromatic driving. Furthermore, as the positions of the observed resonance anticrossings are predictable from the qubit parameters, we envision that, while on the one hand these can be exploited for the operation of dressed semiconductor qubits, on the other hand, these frequencies should be avoided when implementing bichromatic EDSR. Future experiments may focus on the optimization of bichromatic driving, for example, by tuning parameters such as the

interdot coupling, aiming to achieve high-fidelity control of large qubit arrays.

All data and analysis underlying this study are available on a 4TU.ResearchData repository [40].

*These authors contributed equally to this work.

[1] A. Chatterjee, P. Stevenson, S. De Franceschi, A. Morello, N. P. de Leon, and F. Kuemmeth, Semiconductor qubits in practice, Nat. Rev. Phys. **3**, 157 (2021).

[2] G. Burkard, T. D. Ladd, A. Pan, J. M. Nichol, and J. R. Petta, Semiconductor spin qubits, Rev. Mod. Phys. **95**, 025003 (2023).

[3] L. M. K. Vandersypen, H. Bluhm, J. S. Clarke, A. S. Dzurak, R. Ishihara, A. Morello, D. J. Reilly, L. R. Schreiber, and M. Veldhorst, Interfacing spin qubits in quantum dots and donors—hot, dense, and coherent, npj Quantum Inf. **3**, 34 (2017).

[4] D. P. Franke, J. S. Clarke, L. M. Vandersypen, and M. Veldhorst, Rent's rule and extensibility in quantum computing, Microprocessors Microsyst. **67**, 1 (2019).

[5] R. Li, L. Petit, D. P. Franke, J. P. Dehollain, J. Helsen, M. Steudtner, N. K. Thomas, Z. R. Yoscovits, K. J. Singh, S. Wehner, L. M. K. Vandersypen, J. S. Clarke, and M. Veldhorst, A crossbar network for silicon quantum dot qubits, Sci. Adv. **4**, eaar3960 (2018).

[6] F. Borsoi, N. W. Hendrickx, V. John, M. Meyer, S. Motz, F. van Riggelen, A. Sammak, S. L. de Snoo, G. Scappucci, and M. Veldhorst, Shared control of a 16 semiconductor quantum dot crossbar array, Nat. Nanotechnol. (2023).

[7] Z. György, A. Pályi, and G. Széchenyi, Electrically driven spin resonance with bichromatic driving, Phys. Rev. B **106**, 155412 (2022).

[8] W. A. Coish and D. Loss, Exchange-controlled single-electron-spin rotations in quantum dots, Phys. Rev. B **75**, 161302(R) (2007).

[9] E. A. Laird, C. Barthel, E. I. Rashba, C. M. Marcus, M. P. Hanson, and A. C. Gossard, A new mechanism of electric dipole spin resonance: Hyperfine coupling in quantum dots, Semicond. Sci. Technol. **24**, 064004 (2009).

[10] E. I. Rashba, Mechanism of half-frequency electric dipole spin resonance in double quantum dots: Effect of nonlinear charge dynamics inside the singlet manifold, Phys. Rev. B **84**, 241305(R) (2011).

[11] P. Scarlino, E. Kawakami, D. R. Ward, D. E. Savage, M. G. Lagally, M. Friesen, S. N. Coppersmith, M. A. Eriksson, and L. M. K. Vandersypen, Second-harmonic coherent driving of a spin qubit in a Si/SiGe quantum dot, Phys. Rev. Lett. **115**, 106802 (2015).

[12] J. Romhányi, G. Burkard, and A. Pályi, Subharmonic transitions and Bloch-Siegert shift in electrically driven spin resonance, Phys. Rev. B **92**, 054422 (2015).

[13] K. Takeda, J. Yoneda, T. Otsuka, T. Nakajima, M. R. Delbecq, G. Allison, Y. Hoshi, N. Usami, K. M. Itoh, S. Oda, T. Kodera, and S. Tarucha, Optimized electrical control of a Si/SiGe spin qubit in the presence of an induced frequency shift, npj Quantum Inf. **4**, 54 (2018).

[14] B. Undseth, X. Xue, M. Mehmandoost, M. Russ, N. Samkharadze, A. Sammak, V. V. Dobrovitski, G. Scappucci, and L. M. K. Vandersypen, Nonlinear response and crosstalk of strongly driven silicon spin qubits, Phys. Rev. Appl. **19**, 044078 (2023).

[15] W. Gilbert *et al.*, On-demand electrical control of spin qubits, Nat. Nanotechnol. **18**, 131 (2023).

[16] S. Bosco, S. Geyer, L. C. Camenzind, R. S. Eggli, A. Fuhrer, R. J. Warburton, D. M. Zumbühl, J. C. Egues, A. V. Kuhlmann, and D. Loss, Phase-driving hole spin qubits, Phys. Rev. Lett. **131**, 197001 (2023).

[17] H. Levine, A. Keesling, A. Omran, H. Bernien, S. Schwartz, A. S. Zibrov, M. Endres, M. Greiner, V. Vuletić, and M. D. Lukin, High-fidelity control and entanglement of Rydberg-atom qubits, Phys. Rev. Lett. **121**, 123603 (2018).

[18] S. Ebadi, T. T. Wang, H. Levine, A. Keesling, G. Semeghini, A. Omran, D. Bluvstein, R. Samajdar, H. Pichler, W. W. Ho, S. Choi, S. Sachdev, M. Greiner, V. Vuletić, and M. D. Lukin, Quantum phases of matter on a 256-atom programmable quantum simulator, Nature (London) **595**, 227 (2021).

[19] J. A. Valery, S. Chowdhury, G. Jones, and N. Didier, Dynamical sweet spot engineering via two-tone flux modulation of superconducting qubits, PRX Quantum **3**, 020337 (2022).

[20] N. W. Hendrickx, W. I. Lawrie, M. Russ, F. van Riggelen, S. L. de Snoo, R. N. Schouten, A. Sammak, G. Scappucci, and M. Veldhorst, A four-qubit germanium quantum processor, Nature (London) **591**, 580 (2021).

[21] M. Lodari, N. W. Hendrickx, W. I. L. Lawrie, T.-K. Hsiao, L. M. K. Vandersypen, A. Sammak, M. Veldhorst, and G. Scappucci, Low percolation density and charge noise with holes in germanium, Mater. Quantum Technol. **1**, 011002 (2021).

[22] See Supplemental Material at http://link.aps.org/supplemental/10.1103/PhysRevLett.132.067001 for supplemental experimental data, methods, and a full derivation of the theoretical model, which includes Refs. [23–28].

[23] R. Winkler, Quasi-degenerate perturbation theory, in *Spin-Orbit Coupling Effects in Two-Dimensional Electron and Hole Systems* (Springer, New York, 2003), pp. 201–205.

[24] J. H. Shirley, Solution of the Schrödinger equation with a Hamiltonian periodic in time, Phys. Rev. **138**, B979 (1965).

[25] T.-S. Ho, S.-I. Chu, and J. V. Tietz, Semiclassical many-mode Floquet theory, Chem. Phys. Lett. **96**, 464 (1983).

[26] J. R. Schrieffer and P. A. Wolff, Relation between the Anderson and Kondo Hamiltonians, Phys. Rev. **149**, 491 (1966).

[27] Y. Kato, R. Myers, D. Driscoll, A. Gossard, J. Levy, and D. Awschalom, Gigahertz electron spin manipulation using voltage-controlled *g*-tensor modulation, Science **299**, 1201 (2003).

[28] A. Crippa, R. Maurand, L. Bourdet, D. Kotekar-Patil, A. Amisse, X. Jehl, M. Sanquer, R. Laviéville, H. Bohuslavskyi, L. Hutin *et al.*, Electrical spin driving by *g*-matrix modulation in spin-orbit qubits, Phys. Rev. Lett. **120**, 137702 (2018).

[29] T. Hensgens, T. Fujita, L. Janssen, X. Li, C. J. Van Diepen, C. Reichl, W. Wegscheider, S. Das Sarma, and L. M. K. Vandersypen, Quantum simulation of a Fermi–Hubbard model using a semiconductor quantum dot array, Nature (London) **548**, 70 (2017).

[30] W. I. L. Lawrie, N. W. Hendrickx, F. van Riggelen, M. Russ, L. Petit, A. Sammak, G. Scappucci, and M. Veldhorst, Spin relaxation benchmarks and individual qubit addressability for holes in quantum dots, Nano Lett. **20**, 7237 (2020).

[31] M. Baur, S. Filipp, R. Bianchetti, J. M. Fink, M. Göppl, L. Steffen, P. J. Leek, A. Blais, and A. Wallraff, Measurement of Autler-Townes and Mollow transitions in a strongly driven superconducting qubit, Phys. Rev. Lett. **102**, 243602 (2009).

[32] M. A. Sillanpää, J. Li, K. Cicak, F. Altomare, J. I. Park, R. W. Simmonds, G. S. Paraoanu, and P. J. Hakonen, Autler-Townes effect in a superconducting three-level system, Phys. Rev. Lett. **103**, 193601 (2009).

[33] I. Hansen, A. E. Seedhouse, K. W. Chan, F. E. Hudson, K. M. Itoh, A. Laucht, A. Saraiva, C. H. Yang, and A. S. Dzurak, Implementation of an advanced dressing protocol for global qubit control in silicon, Appl. Phys. Rev. **9**, 031409 (2022).

[34] A. Laucht, R. Kalra, S. Simmons, J. P. Dehollain, J. T. Muhonen, F. A. Mohiyaddin, S. Freer, F. E. Hudson, K. M. Itoh, D. N. Jamieson, J. C. McCallum, A. S. Dzurak, and A. Morello, A dressed spin qubit in silicon, Nat. Nanotechnol. **12**, 61 (2017).

[35] K. C. Miao, J. P. Blanton, C. P. Anderson, A. Bourassa, A. L. Crook, G. Wolfowicz, H. Abe, T. Ohshima, and D. D. Awschalom, Universal coherence protection in a solid-state spin qubit, Science **369**, 1493 (2020).

[36] B. Martinez, J. C. Abadillo-Uriel, E. A. Rodríguez-Mena, and Y.-M. Niquet, Hole spin manipulation in inhomogeneous and nonseparable electric fields, Phys. Rev. B **106**, 235426 (2022).

[37] M. Russ, D. M. Zajac, A. J. Sigillito, F. Borjans, J. M. Taylor, J. R. Petta, and G. Burkard, High-fidelity quantum gates in Si/SiGe double quantum dots, Phys. Rev. B **97,** 085421 (2018).

[38] N. W. Hendrickx, L. Massai, M. Mergenthaler, F. Schupp, S. Paredes, S. W. Bedell, G. Salis, and A. Fuhrer, Sweet-spot operation of a germanium hole spin qubit with highly anisotropic noise sensitivity, arXiv:2305.13150.

[39] A. Sarkar, Z. Wang, M. Rendell, N. W. Hendrickx, M. Veldhorst, G. Scappucci, M. Khalifa, J. Salfi, A. Saraiva, A. S. Dzurak, A. R. Hamilton, and D. Culcer, Electrical operation of planar Ge hole spin qubits in an in-plane magnetic field, arXiv:2307.01451.

[40] V. John *et al.*, Raw data, analysis and modelling scripts for the article "Bichromatic Rabi control of semiconductor qubits." Version 1. 4TU. ResearchData, dataset (2023), 10.4121/bb43fe1d-f503-49e8-9f17-ce7d734f015d.